



**Shapiro steps and chaos in the Frenkel-Kontorova model with substrate lateral vibration**Yongfeng Wei <sup>1</sup> and Youming Lei <sup>1,2,\*</sup><sup>1</sup>*School of Mathematics and Statistics, Northwestern Polytechnical University, Xi'an 710072, China*<sup>2</sup>*Ministry of Industry and Information Technology Key Laboratory of Dynamics and Control of Complex Systems, Northwestern Polytechnical University, Xi'an, 710072, China*

(Received 22 June 2022; accepted 27 September 2022; published 12 October 2022)

Numerical simulations are used to examine the dynamics of the dc-driven Frenkel-Kontorova model with an oscillation substrate subjected to lateral periodic excitations in overdamped and underdamped cases, respectively. The results reveal that the system exhibits frequency locking and chaotic behaviors due to the fact that the lateral vibration of the substrate potential introduces an additional frequency and degree of freedom into the system. In the overdamped case, we show that the appearance of subharmonic Shapiro steps can be attributed to the deformation of the substrate potential or inertia. The characteristics of the steps are significantly affected by the amplitude and frequency of the lateral vibration. When the vibration frequency is relatively high, the change of the width of the first harmonic Shapiro step with increasing amplitude exhibits a Bessel-type oscillation, but the oscillation deviates from the Bessel curve at lower frequencies. In the amplitude dependence, although the oscillatory behavior of the critical depinning force at the high frequency is anomalous, local maxima (minima) of the first step width correspond to local minima (maxima) of the critical depinning force, and the largest Lyapunov exponent obtained in the pinned state represents a mirror relationship of the critical depinning force. In contrast to the overdamped system, the underdamped one exhibits both subharmonic Shapiro steps and chaotic behaviors. We show the increased inertia of the latter system plays an important role in suppressing the emergence of subharmonic steps, which is opposite to the result of the former. When the dc force changes, chaos appears not only between adjacent subharmonic Shapiro steps but also on some specific steps where chaos should be avoided. The variation regularity of the first step width and the critical depinning force is thus annihilated in vibration amplitude and frequency dependence. However, superlubricity can be achieved by careful adjustment of vibration amplitude and frequency. The findings can serve as a theoretical guideline for technological applications such as device building and voltage standards.

DOI: [10.1103/PhysRevE.106.044204](https://doi.org/10.1103/PhysRevE.106.044204)**I. INTRODUCTION**

Frequency-locking phenomena are the important characteristics of nonlinear dynamical systems with competing timescales, and one particular phenomenon among them is the occurrence of Shapiro steps [1]. Since the first discovery of Shapiro steps in Josephson junctions, the dynamical mode-locking phenomena have been extensively explored in various systems of coupled oscillators, such as charge-density wave and spin-density wave systems [2,3], irradiated Josephson junctions [4], vortex matter [5], superconducting nanowires [6], skyrmion dynamics [7], and driven colloids [8]. Among these many-body systems, the Frenkel-Kontorova (FK) model [9] is one of the simplest models that can capture the essence of frequency locking well. Despite its simplicity, the FK model exhibits rich and complex dynamic behaviors [10–12] and has been widely used to describe the dynamics of various nonlinear systems [4,9,13–15].

The standard FK model depicts a discrete chain of atoms that are harmonically coupled with their nearest neighbors and subjected to an external sinusoidal substrate potential. Due

to the competition between the equilibrium distance related to the interparticle interaction and the period of substrate potential, the model features both commensurate and incommensurate structures, which display rich dynamical behaviors when they are driven by external forces [16]. When the FK model is driven only by a dc force, there exists a critical depinning force  $F_c$ , also known as the static friction force [17,18], which separates the pinned and the sliding regions of the system. When the FK model is driven by both dc and ac forces, Floría and Falo [13,19,20] investigated it in detail using molecular-dynamics simulations. They found that in commensurate structures, Shapiro steps appear in the curve of the response functions, with the average velocity as a function of the average external driving force [16]. The occurrence of the steps is due to the dynamical mode locking of the internal frequency of the motion of particles over the sinusoidal substrate potential with the frequency of the external periodic force.

The FK model reveals some interesting results regarding the harmonic and subharmonic Shapiro steps. For the standard dissipative FK model with commensurate structures driven by external periodic forces, as the ac force amplitude increases, the first harmonic step width and the critical depinning force show Bessel-type oscillatory behaviors at high frequencies,

\*Corresponding author: [leiyuming@nwpu.edu.cn](mailto:leiyuming@nwpu.edu.cn)

and local maxima (minima) of the former correspond to local minima (maxima) of the latter [21,22]. However, the model with integer values of winding number cannot be used to research phenomena associated with subharmonic steps since they do not exist in this case [23,24], and the steps size is too small for reasonable noninteger values to analyze their existence and properties [13,19]. Further investigation demonstrates that the largest Lyapunov exponent (LLE) [25] is a very sensitive method for detecting any harmonic and subharmonic steps. Additionally, it can detect the presence of chaos. When the Shapiro steps are present, the LLE of the system is negative, whereas a positive LLE is always indicative of chaos [13,19]. More interestingly, the amplitude dependence of the LLE in the pinned state where the dc force  $F_{dc} = 0$  shows a mirror image of the critical depinning force amplitude dependence, and this feature persists when the interparticle potential is exponential [22,26], which points out an advantage of the LLE computation. Different from the standard dc- and ac-driven FK model, when the substrate potential has deformation, a series of large subharmonic steps appear in the system with any commensurate structure, and their appearance obeys the Farey sequence [27]. With the change of deformation parameters, anomalies occur in the amplitude dependence of the Shapiro steps width and the critical depinning force, which deviate from the well-known Bessel-type behavior [27–30]. The anomalies also appear in incommensurate structures due to the broken symmetry of particle motion [31]. All of these studies demonstrate that neither commensurate nor incommensurate structures of the dissipative FK model with convex interparticle potentials or deformable substrate potentials exhibit chaos [26,27], which can be attributed to the Middleton’s no passing rule [32,33]. When the FK model includes an inertial term, unlike in the overdamped case, the most striking inertial effect is the appearance of chaotic behaviors, and with the change of mass, the subharmonic steps are separated by chaotic windows, while the whole structure retains the scale similarity of the original staircase [34,35].

In the dc- and ac-driven FK model, most of the studies focus on harmonic or deformable substrate potentials, while the substrate potential with vibration has seldom been examined. When the system is affected by internal and external factors, vibration often occurs, which is widely studied in many fields. For instance, energy can be harvested from vibrations in energy harvesting systems, and vibrational energy harvesters usually feature low damping ratios to maximize the harvested power at resonance [36]. The study of dissipative dynamics of a particle subjected to a lateral vibrational periodic potential demonstrates that chaos can be induced by the potential [37]. In a Bose-Einstein condensate [38], Azizi and Valizadeh considered using a laterally vibrating shallow optical lattice to explore the dynamics of a bright soliton. They showed that the phase space of the equation of motion for the center of mass of the soliton exhibits multistability or chaos depending on the parameters, amplitude, and frequency of the vibration of the lattice. In the model of an atomic force microscopy tip interacting with a substrate that oscillates in the lateral direction, the surface diffusivity and mobility of the systems are significantly increased [39–42]. Therefore, it is possible to reduce the friction of the system by adjusting the amplitude and frequency of the vibration. According to the previous

studies [39–41], the substrate vibration can be transformed into ac forces, leading two competing frequencies to exist in the FK model driven by the dc force, which may result in the appearance of Shapiro steps. Additionally, the vibration has a positive effect on the nanofriction phenomenon, which is associated with the critical depinning force of the system. Therefore, it is important to investigate the effect of the substrate vibration on the dynamic behaviors of the dc-driven FK model.

In general, the existence and robustness (structural stability) of Shapiro steps with the change of system parameters has attracted much interest in the research of the dc- and ac-driven systems. The purpose of this work is to explore the influence of the amplitude and frequency of the substrate vibration on the Shapiro steps and the critical depinning force of the dc-driven FK model. We will use the response functions, the LLE, and the bifurcation diagram of the Poincaré section to study the phenomena of harmonic steps, subharmonic steps, and chaos in the dc-driven FK model with lateral excitations of the substrate potential. The rest of the paper is organized as follows. A brief description of the FK model with substrate lateral vibration is introduced in Sec. II. The dependence of Shapiro steps, critical depinning force, and chaos on the substrate vibration in the FK model under both overdamped and underdamped cases are examined with numerical simulations in Sec. III. Section IV concludes the paper.

## II. FK MODEL WITH SUBSTRATE LATERAL VIBRATION

The total potential energy of the standard FK model is [13]

$$H = \sum_j [V(u_j) + W(u_{j+1} - u_j)], \quad j = 1, 2, \dots, N, \quad (1)$$

where  $N$  is the number of particles. The substrate potential  $V(u_j)$  is defined as

$$V(u_j) = \frac{K}{(2\pi)^2} [1 - \cos(2\pi u_j)], \quad (2)$$

where  $K$  is the pinning strength, and  $W(u_{j+1} - u_j)$  is a function of the distance between adjacent particles, in which the harmonic interparticle potential is considered with the following form:

$$W(u_{j+1} - u_j) = \frac{1}{2}(u_{j+1} - u_j)^2. \quad (3)$$

We take account into the effect of the vibration on the dynamic behaviors of the FK model by applying a lateral periodic excitation  $f(t) = A \cos(2\pi \nu_0 t)$  to the substrate potential, which is similar to that in Ref. [37]. That is, the substrate potential of the system can be written as

$$\begin{aligned} V(u_j, t) &= \frac{K}{(2\pi)^2} (1 - \cos\{2\pi[u_j - f(t)]\}) \\ &= \frac{K}{(2\pi)^2} (1 - \cos\{2\pi[u_j - A \cos(2\pi \nu_0 t)]\}), \end{aligned} \quad (4)$$

where  $A$  and  $\nu_0$  are the amplitude and frequency of the vibration, respectively.

The FK model with substrate lateral vibration is driven by the dc external force  $F_{dc}$ , and the equation of motion is

$$\ddot{u}_j = -\frac{K}{2\pi} \sin\{2\pi[u_j - A \cos(2\pi\nu_0 t)]\} + u_{j+1} + u_{j-1} - 2u_j - \gamma\dot{u}_j + F_{dc}, \quad (5)$$

where  $j = 1, 2, \dots, N$ ,  $u_j$  is the position of  $j$ th particle, and  $\gamma$  is the damping coefficient. For some constant force  $F_{dc}$ , the system is overdamped when (see the specific derivation in Ref. [34])

$$\gamma > \sqrt{4(2+K)}. \quad (6)$$

Use variable substitutions

$$w_j = u_j - A \cos(2\pi\nu_0 t), \quad (7)$$

then Eq. (5) is equivalent to

$$\ddot{w}_j = -\frac{K}{2\pi} \sin(2\pi w_j) + w_{j+1} + w_{j-1} - 2w_j - \gamma\dot{w}_j + A(2\pi\nu_0)^2 \cos(2\pi\nu_0 t) + 2\pi\nu_0\gamma A \sin(2\pi\nu_0 t) + F_{dc}, \quad (8)$$

which can be rewritten as

$$\ddot{w}_j = -\frac{K}{2\pi} \sin(2\pi w_j) + w_{j+1} + w_{j-1} - 2w_j - \gamma\dot{w}_j + F_{ac} \cos(2\pi\nu_0 t - \varphi) + F_{dc}, \quad (9)$$

where  $F_{ac} = 2\pi\nu_0 A \sqrt{(2\pi\nu_0)^2 + \gamma^2}$ ,  $\varphi = \arctan(\frac{\gamma}{2\pi\nu_0})$ .

In Eq. (9) the model is driven by dc and ac forces, resulting in two frequency scales: one is the frequency of the particle motion associated with sinusoidal substrate potential and the other is the frequency of the ac force  $\nu_0$ . Due to the competition of these two different frequency scales, the Shapiro steps may appear in the system. When the locking appears at integer multiples of frequency, the steps are harmonic, whereas at rational noninteger multiples of frequency, they are subharmonic. These steps correspond to resonant solutions of Eq. (5). If  $\{u_j(t)\}$  is a steady-state solution of Eq. (5), then

$$\sigma_{l,m,s}\{u_j(t)\} = \left[ u_{j+l} \left( t - \frac{s}{\nu_0} \right) + m \right] = \{u'_j(t)\}, \quad (10)$$

is another steady-state solution of the equation, where  $l$ ,  $m$ , and  $s$  are arbitrary integers.

Since

$$\sin\{2\pi[u'_j(t) - A \cos(2\pi\nu_0 t)]\} = \sin\left\{2\pi\left[u_{j+l}\left(t - \frac{s}{\nu_0}\right) - A \cos(2\pi\nu_0 t)\right]\right\}, \quad (11)$$

the effectiveness of the transformation (10) can be verified.

If the solution is invariant under the symmetry operation (10), it is called resonant. The corresponding time average velocity [13] satisfies

$$\bar{v} = \left\langle \frac{1}{N} \sum_{j=1}^N \dot{u}_j \right\rangle_t = \frac{l\omega + m}{s} \nu_0, \quad (12)$$

where  $\langle \rangle_t$  means averaging over time,  $\omega = \langle (u_{j+1} - u_j) \rangle$  is the average distance between particles, i.e., the winding number. The system has commensurate structures when  $\omega$  is rational, while it has incommensurate structures when  $\omega$  is irrational.  $s$  represents the period of the solution. When  $s = 1$ , the resonant solutions or Shapiro steps are called harmonic steps, while the steps are called subharmonic steps when  $s > 1$ .

In the commensurate structures, the resonant velocity (12) can be simplified into the form

$$\bar{v} = \frac{l}{s} \omega \nu_0, \quad (13)$$

where  $\frac{l}{s} = \frac{1}{1}, \frac{2}{1}, \frac{3}{1}, \dots$  marks the first, second, and third harmonic steps, and  $\frac{l}{s} = \frac{1}{2}, \frac{3}{2}, \frac{5}{2}, \dots, \frac{1}{3}, \frac{2}{3}, \frac{4}{3}, \dots, \frac{1}{4}, \frac{3}{4}, \frac{5}{4}, \dots$ , marks the subharmonic steps.

In the FK model driven by dc and ac forces, the appearance of Shapiro steps always follows a specific order, and all the observed subharmonic steps belong to the Farey sequences without exceptions [27]. To analyze the observed harmonic and subharmonic steps, an algorithm proposed in Ref. [43] is used in this study. With this method, the Shapiro steps of the staircase structure can be described by a continued fraction formula [30,44,45], and the average velocity is

$$\bar{v} = \left( i \pm \frac{1}{m \pm \frac{1}{n \pm \frac{1}{p \pm \dots}}} \right) \omega \nu_0, \quad (14)$$

where  $i$ ,  $m$ ,  $n$ ,  $p$  are positive integers. The first-level terms relate to  $i$  describe the harmonic steps, while the other terms represent the subharmonic steps.

In this work, we study only the dynamics of the system with the commensurate structure, where the average distance between particles is  $\omega = 1/2$ . The fourth-order Runge-Kutta method is implemented to obtain the response functions of Eq. (5) with the periodic boundary conditions. In simulations, the time step is  $\Delta t = 0.01\tau$ , where  $\tau = 1/\nu_0$ , and for each value of  $F_{dc}$ , Eq. (5) is integrated for a time of  $T_0 = 400\tau$  to reach a steady state. Although the winding number  $\omega$  is not explicitly included in Eq. (5), it is important. When the external dc force is zero, the system is initialized with all particles at rest and the spacing of two adjacent particles is  $\omega$ . The initial condition is  $u_j = -\frac{N-1}{2}\omega + j\omega$ , where  $j = 1, 2, \dots, N$ , and  $N = 8$ . The periodic boundary conditions are  $u_0 = u_N - N\omega$  and  $u_{N+1} = u_1 + N\omega$ . The dc force is varied adiabatically from zero in steps ranging from  $\Delta F_{dc} = 10^{-4}$  to  $10^{-5}$ . In addition to the response functions, the LLE  $\lambda$  is calculated according to the Wolf algorithm [46].

### III. RESULTS

In this section we shall concentrate on dynamic behaviors of the dc-driven FK model with substrate subjected to a lateral periodic vibration for the overdamped and underdamped cases by using the response functions, the LLE, and the bifurcation diagram of the Poincaré section, respectively.

#### A. Dynamic behaviors of overdamped system

First, we investigate the dynamics of the overdamped case where the damping coefficient can be chosen as  $\gamma = 5$

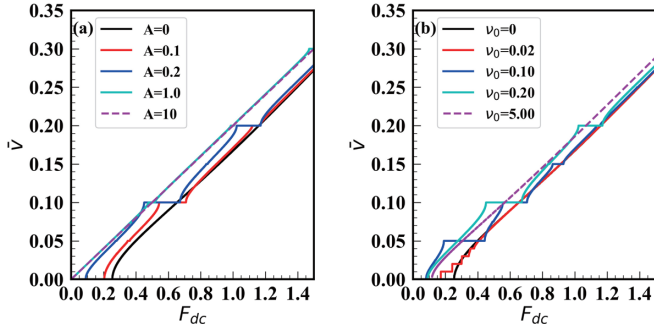


FIG. 1. Average velocity  $\bar{v}$  as a function of the dc force  $F_{dc}$  for  $\omega = 1/2$ ,  $K = 4$ ,  $\gamma = 5$ , in different vibration amplitude and frequency regions: (a)  $\nu_0 = 0.20$  and  $A = 0, 0.1, 0.2, 1.0, 10$ , and (b)  $A = 0.2$  and  $\nu_0 = 0, 0.02, 0.10, 0.20, 5.00$ .

according to Eq. (6). Here we analyze the characteristics of the response functions, the first harmonic step width, the critical depinning force, and the LLE in the pinned state where the dc force  $F_{dc} = 0$  with the change of the vibration amplitude and frequency.

The response functions  $\bar{v}(F_{dc})$  of Eq. (5) are presented in Fig. 1. In Fig. 1(a) we investigate the effects of substrate lateral vibration amplitude  $A$  on response functions when the vibration frequency is fixed as  $\nu_0 = 0.20$ . If the amplitude of the vibration  $A = 0$ , Eq. (5) is a standard overdamped FK model driven only by the dc force, so there are no competing timescales, thus not permitting Shapiro steps to appear in the response function. For the dc-driven FK model, the critical depinning force  $F_c$  is also called the dynamical dc threshold  $F_{c0}$ , which is determined by commensurability of the system and properties of the substrate potential [14], and in this case the threshold value is  $F_{c0} = 0.2545$ . When the amplitude increases to  $A = 0.1$ , the response function starts to deviate from the case where  $A = 0$ , and the harmonic steps and the half-integer step  $1/2$  appear in the curve of the response function. At the same time, the critical depinning force becomes smaller, indicating a reduction in friction. When the deformation of the substrate increases, i.e., the amplitude of the vibration increases to  $A = 0.2$ , another half-integer step  $3/2$  appears in the system and the size of the harmonic steps increases. Meanwhile, the critical depinning force is greatly reduced. With the further increase of amplitude, the subharmonic steps almost disappear for  $A = 1.0$  in the response function, and the critical depinning force of the system is nearly zero. In the case of  $A = 10$ , the Shapiro steps and the critical depinning force completely vanish. Figure 1(a) clearly shows that the Shapiro steps can only exist in a specific vibration amplitude region. When  $A \rightarrow 0$ , the system behaves as a dc-driven overdamped system, and when amplitude  $A$  becomes much larger, it behaves like a frictionless system composed of free particles where the Shapiro steps are absent and the critical depinning force tends to zero. For the latter case, we can observe that the size of subharmonic steps becomes very small, even negligible.

In Eq. (9) the amplitude of the ac force  $F_{ac}$  is not only related to the amplitude of the vibration  $A$  but also to the frequency  $\nu_0$ . Figure 1(b) depicts the influence of vibration frequency  $\nu_0$  on response functions for the vibration

amplitude  $A = 0.2$ . In Fig. 1(b) we observe that when the vibration frequency  $\nu_0 = 0$ , i.e., no ac forces in the system, the response function is the same as that of the amplitude  $A = 0$  in Fig. 1(a). When the frequency is very low,  $\nu_0 = 0.02$ , a series of harmonic steps appear at integer multiples of  $\omega\nu_0$ , and the width of harmonic steps is limited in a small interval and the critical depinning force is relatively large. When the frequency increases to  $\nu_0 = 0.10$ , the width of harmonic steps becomes larger and the critical depinning force becomes smaller. As the frequency further increases to  $\nu_0 = 0.20$ , we observe that besides harmonic steps, half-integer steps  $1/2$  and  $3/2$  appear in the response function. In particular, the width of the first harmonic step shrinks instead while the critical depinning force changes to be larger. If the frequency is very high, such as  $\nu_0 = 5.00$ , the system has no Shapiro steps and the response function is similar to that of the dc-driven model, this may be because the particles cannot follow the vibration of the substrate and become insensitive to it. From Fig. 1(b) we can see that the Shapiro steps can only exist in a specific vibration frequency region. With a lower frequency, steps appear only at the lower values of the dc force. If the frequency becomes much larger, the system behaves like a dc-driven system while its average velocity  $\bar{v}$  is larger than that of the dc-driven system.

Figure 1 indicates that in the FK model with substrate lateral vibration dynamical mode locking can occur even in the absence of an explicit, external ac force or radiation, which is the key factor for frequency locking. Namely, lateral vibration of the substrate potential introduces additional frequency and an additional degree of freedom into the system, which can result in frequency locking. Meanwhile, the appearance and size of the steps, as well as the value of the critical depinning force, are affected by the amplitude and frequency of vibration.

### 1. Subharmonic steps in overdamped system

Figure 1 shows that the appearance of subharmonic steps in the system may be attributed to the deformation of the substrate, while the origin of subharmonic steps is still a matter of debate in the frequency-locking systems [16]. Therefore, it is essential to explore the origin of subharmonic steps in the overdamped FK model with substrate lateral vibration. We use the method of LLE because it can sensitively detect the presence of any harmonic or subharmonic steps as well as providing a quantitative measure of the existence of chaos.

Usually the amplitude of the lateral periodic excitations of the substrate may be small enough, so the average velocity of the system and the corresponding LLE as functions of the dc force for  $A = 0.05$  are illustrated in Fig. 2. We can see that the onstep LLE is negative on the harmonic steps 1 and 2, meaning that particles move periodically with time evolution. When the system stays outside the steps, the LLE is nearly zero, indicating that the trajectories of particles are periodic or quasiperiodic [19,25]. That is, no chaotic phenomenon appears in this case. Furthermore, the zoomed segment of Fig. 2(a) depicted in Fig. 2(b) shows that the LLE sensitively detects the half-integer step  $1/2$  and the subharmonic step  $1/3$  that are difficult to observe with the method of the response function. More importantly, the absence of subharmonic steps between the harmonic steps 1 and 2 at this resolution is

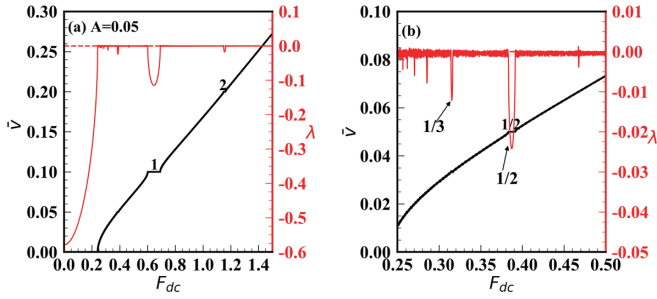


FIG. 2. (a) Average velocity  $\bar{v}$  and the corresponding LLE  $\lambda$  as functions of the dc force  $F_{dc}$  for  $A = 0.05$ . (b) Zoomed segment of (a). The other parameters are the same as in Fig. 1(a). The dotted line represents the curve with LLE  $\lambda = 0$ .

confirmed by magnifying the region between the two steps with the method of the LLE. When the amplitude increases to  $A = 0.2$ , in Fig. 3 we show there is no chaos in the system. In Fig. 3(b) we can also observe that the subharmonic steps  $3/2$ ,  $4/3$ ,  $5/3$  appear between the harmonic Shapiro steps 1 and 2. Comparing Fig. 2 with Fig. 3, we can conclude that the larger deformation of the substrate contributes to the appearance of new subharmonic steps  $3/2$ ,  $4/3$ ,  $5/3$ , which is similar to the results in Ref. [28]. On the other hand, if the damping in Fig. 3(b) increases to  $\gamma = 7$  while the other parameters remain unchanged, we can obtain that there is only the subharmonic step  $3/2$  between the harmonic Shapiro steps 1 and 2, and the higher order subharmonic steps  $4/3$ ,  $5/3$  disappear. Since the decrease of damping corresponds to an increase of inertia in the system, the increased inertia plays an important role in inducing the emergence of subharmonic steps in the overdamped system. Therefore, the appearance of subharmonic steps can be attributed to deformation or inertia in the overdamped FK system with substrate lateral vibration. And the system does not exhibit a chaotic behavior as the motion of the system follows the Middleton no-passing rule. According to this rule, the order between the particles must be preserved, i.e., at any point in time, a larger solution cannot be crossed by a smaller one [16].

## 2. Influence of vibration amplitude

Figures 1–3 indicate the lateral vibration strongly influences the Shapiro steps and the critical depinning force. To

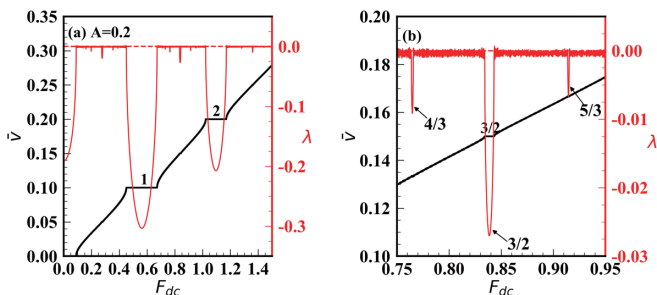


FIG. 3. (a) Average velocity  $\bar{v}$  and the corresponding LLE  $\lambda$  as functions of the dc force  $F_{dc}$  for  $A = 0.2$ . (b) Zoomed segment of (a). The other parameters are the same as in Fig. 1(a). The dotted line represents the curve with LLE  $\lambda = 0$ .

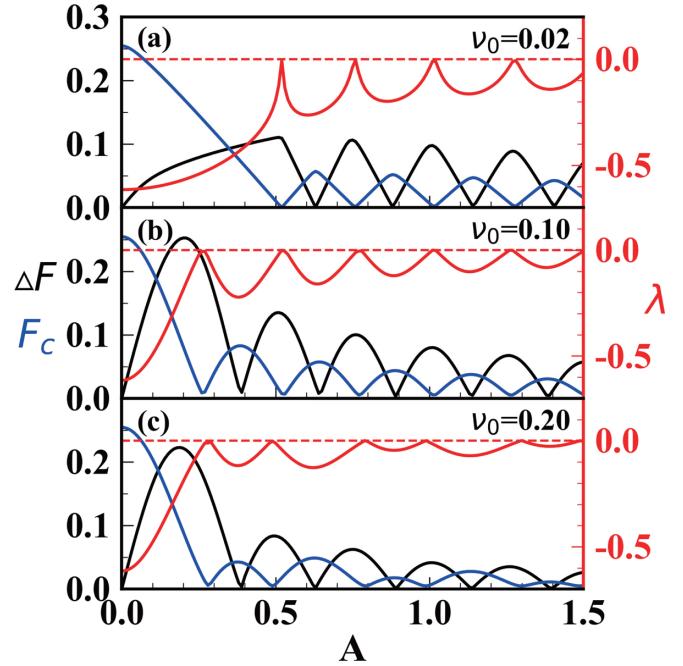


FIG. 4. The width of the first harmonic step  $\Delta F$ , the critical depinning force  $F_c$ , and the LLE  $\lambda$  in the pinned state ( $F_{dc} = 0$ ) as functions of the vibration amplitude  $A$  for different values of frequency: (a)  $\nu_0 = 0.02$ , (b)  $\nu_0 = 0.10$ , (c)  $\nu_0 = 0.20$ . The dotted line represents the curve with LLE  $\lambda = 0$ .

provide more insight into the effect of vibration amplitude, the width  $\Delta F$  of the first harmonic step  $\bar{v} = \omega\nu_0$  and the critical depinning force  $F_c$  as functions of the amplitude for three different values of vibration frequency are presented in Fig. 4. As we can see in Fig. 4,  $\Delta F$  and  $F_c$  exhibit distinct oscillatory behaviors for different values of frequency with increasing amplitude. In Fig. 4(a) at a relatively low frequency  $\nu_0 = 0.02$ , the maximum step width (the first maximum of the curve  $\Delta F$ ) [21] of value  $\Delta F \approx 0.1106$  is very low and the difference between the first maximum and the other local maxima is not so pronounced. With the increase of frequency to  $\nu_0 = 0.10$ , the maximum step width  $\Delta F \approx 0.2524$  increases significantly, shown in Fig. 4(b). It is the highest one compared to the cases in Figs. 4(a) and 4(c). Particularly, as the amplitude increases, the oscillation of the step width exhibits a Bessel-type form as the previous study [21] and the peak values of oscillation decrease. At a high frequency  $\nu_0 = 0.20$  in Fig. 4(c), the maximum step width of value  $\Delta F \approx 0.2228$  is slightly reduced compared with the case of  $\nu_0 = 0.10$ , while the oscillation with the increase of amplitude has a similar Bessel-type form as in Fig. 4(b).

When the amplitude of the vibration  $A = 0$ , the critical depinning force reaches the dynamical dc threshold value  $F_{c0} = 0.2545$ , while as  $A$  increases, the critical depinning force exhibits distinct oscillation behaviors in the three frequency regimes. At the low frequency  $\nu_0 = 0.02$  in Fig. 4(a), the critical vibration amplitude  $A \approx 0.52$ , which corresponds to the first minimum of  $F_c$ , is the maximal one in the three cases. With the increase of amplitude  $A$ , there is no significant difference between the other local maximal values of  $F_c$  except for the first maximum of  $F_c$ . When the frequency

increases to  $\nu_0 = 0.10$  in Fig. 4(b), the critical amplitude  $A \approx 0.26$  corresponding to the first minimum of  $F_c$  turns to be much smaller. As the amplitude of the vibration increases, the critical depinning force  $F_c$  exhibits a Bessel-type oscillatory behavior and the local maximal values of  $F_c$  are getting smaller. With the further increase of frequency to  $\nu_0 = 0.20$ , in Fig. 4(c) the amplitude corresponding to the first minimum of  $F_c$  increases to  $A \approx 0.28$  instead, a little larger than the case of  $\nu_0 = 0.10$ . Particularly, Fig. 4(c) reveals the anomalous oscillation behavior of the critical depinning force, in which the odd lobes are larger than the even lobes. This phenomenon also appears in the standard FK model with incommensurate structure [31] and in the FK model with deformable substrate potential [28]. However, they may have different origins. In this work, it may be due to the fact that in the even lobes, the lateral vibration can reduce the bindings of the substrate potential to particles, making it more easily for the particles to move out of the confinement of the potential. In all three cases, we can observe that local maxima (minima) of the first step width  $\Delta F$  correspond to local minima (maxima) of the critical depinning force  $F_c$ .

At the same time, we plot the LLE in Fig. 4 as a function of the amplitude for  $F_{dc} = 0$ , i.e., we consider dynamic convergence and divergence of the FK model with a lateral vibration, but without the application of external dc forces to particles, in order to investigate whether the mirror relationship between the amplitude dependence of LLE in the pinned state ( $F_{dc} = 0$ ) and the dependence of the critical depinning force on the amplitude still exists. As we can see from Fig. 4, the vibration amplitude dependence of the LLE in the pinned state still presents a mirror image of that of the critical depinning force even if the latter has an anomalous oscillation form at the high frequency. The results further verify that the LLE is a convenient tool to study the dynamics of the driven FK model, since we can obtain the properties of Shapiro steps and critical depinning force without actually driving the system, which saves extensive computational effort [22]. In addition, we observe that the LLE in the pinned state is smaller when the amplitude  $A$  of the lateral periodic excitation is very small, indicating that in the absence of an external dc force the smaller the amplitude is, the stabler the system would be.

The oscillation of the step width is determined by the external periodic ac force [21,31]. How does the ac force affect the system? When the velocity of the system reaches the resonant values, the ac force will induce an additional polarization energy which is less than zero into the system, and the average pinning force begins to change from zero. At the resonant values, because the average pinning energy of the system in the locked state (on the step) is lower than that in the unlocked state, the system will be locked. With the increase of the dc force, the system will remain locked until the pinning force can offset the changes of the dc force. Hu and Tekić [21] pointed out that, in the standard FK model, the reason why the first harmonic step width exhibits Bessel-type form oscillatory behaviors with the increase of ac amplitude is that the ac force induces the back and forward displacement of particles. The amplitude of the ac force determines how much this motion is retarded, that is, how many sites the particles will jump backward [16,47,48]. In this study, the lateral vibration of the substrate potential introduces an additional degree of

freedom into the system according to Eqs. (5) and (9), where the lateral vibration can be converted to an ac force similar to that in Ref. [21]. It should be noted, however, the corresponding amplitude  $F_{ac} = 2\pi\nu_0 A \sqrt{(2\pi\nu_0)^2 + \gamma^2}$  in Eq. (9) is affected not only by the vibration amplitude  $A$ , but also by the vibration frequency  $\nu_0$ . Once  $\nu_0$  is fixed, the amplitude  $F_{ac}$  is proportional to  $A$ , which clarifies the reason why the step width oscillates with  $A$  in a way similar to the case of ac-driven FK model. With the vibration amplitude  $A$  increases from zero, corresponding to the values of the first lobe of the step width oscillation, particles oscillate around the bottom of the potential well symmetrically in one motion cycle and then hop to the next site. When  $A$  reaches the value corresponding to the first maximum of the oscillation, particles are pinned most of the time before hopping to the next well. When  $A$  increases to the value corresponding to the first minimum of the oscillation, the motion of particles changes to back and forward jumps in one cycle. For the value corresponding to the second maximum, particles will jump back one site and forward two sites. As the vibration amplitude  $A$  increases, particles hop between the wells far and far away and stay for less and less time pinned, so the step width will decrease gradually in an oscillating manner. The results in Fig. 4 show that the oscillating manner exhibits a Bessel-type curve at relatively high frequencies where the period of the ac force is small. When the vibration frequency increases from  $\nu_0 = 0.10$  in Fig. 4(b) to  $\nu_0 = 0.20$  in Fig. 4(c), the corresponding local maxima of the first step width decrease, which is different from the result of the dc- and ac-driven standard FK model. This may be due to a competition of two effects. The first effect is that the increase of vibration frequency shortens the period of the ac force, causing particles to have insufficient time to move between further wells, hence the width of the steps will increase. The second is that in light of Eq. (9), the increase of vibration frequency is equivalent to the increase of amplitude of ac force in Ref. [21], so that particles move between more distant sites, resulting in a decrease in the width of the step. As a result of competition, the simultaneous influence of the two effects eventually leads to a decrease of the step width with increasing frequency.

### 3. Influence of vibration frequency

We examine the influence of vibration frequency on the first harmonic step width and on the critical depinning force for three different values of amplitude, shown in Fig. 5. When the amplitude of vibration  $A = 0.1$  in Fig. 5(a), the step width first gradually increases with the increase of frequency, and after reaching its maximum  $\Delta F \approx 0.1784$ , slowly decreases towards zero with the further increase of frequency. As the vibration amplitude increases to  $A = 0.2$  in Fig. 5(b), the step width curve follows a nonmonotonic property similar to the case of  $A = 0.1$ , while its initial increase becomes faster, and its maximum  $\Delta F \approx 0.2531$  is the largest one in the three amplitude regions. When the large amplitude  $A = 1.0$  in Fig. 5(c), a richer dynamical behavior emerges: the step width oscillates at low frequencies; as the frequency increases, it first increases to its maximum  $\Delta F \approx 0.0971$ , then decreases sharply to a minimum value; with the further

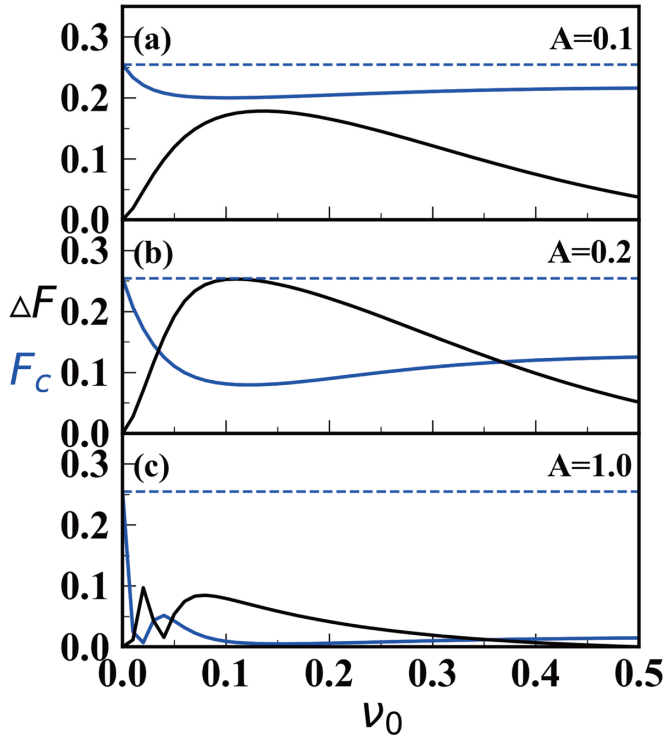


FIG. 5. The width of the first harmonic step  $\Delta F$  and the critical depinning force  $F_c$  as functions of the vibration frequency  $\nu_0$  for different values of amplitude: (a)  $A = 0.1$ , (b)  $A = 0.2$ , (c)  $A = 1.0$ . The dotted curve represents dynamical dc threshold:  $F_{c0} = 0.2545$ . The other parameters are the same as in Fig. 1.

increase of frequency, it increases to a local maximum, and finally decreases to zero.

In Fig. 5 the critical depinning force also exhibits different changing behaviors with the increase of vibration frequency for three amplitude regions. In Fig. 5(a) the critical depinning force  $F_c$  first decreases to its minimum with the increase of frequency, then increases slowly and finally tends to  $F_c \approx 0.2170$ , which is a little smaller than  $F_{c0} = 0.2545$ . In Fig. 5(b) the critical depinning force preserves the previously described behavior in Fig. 5(a), while the speed of decreasing to a smaller minimum becomes higher and  $F_c$  finally tends to  $F_c \approx 0.1260$ , smaller than  $F_{c0} = 0.2545$ , with the further increase of frequency. In Fig. 5(c)  $F_c$  exhibits a reverse oscillatory behavior similar to that of the step width at low frequencies. With the increase of frequency,  $F_c$  first decreases to a local minimum value, then increases to a local maximum; with the further increase of frequency, it gradually decreases to zero, then slowly increases, and finally tends to  $F_c \approx 0.0150$ , far smaller than  $F_{c0} = 0.2545$ . In addition, all of the critical depinning forces in Fig. 5 are smaller than the dynamical dc threshold  $F_{c0} = 0.2545$  once the vibration frequency is larger than zero.

In Fig. 5 we can observe that local maxima (minima) of the step width and local minima (maxima) of the critical depinning force still correspond to each other with the increase of vibration frequency, which is consistent with the conclusion in Fig. 4 and in the standard FK model [21]. We show different changing behaviors although the system considered exhibits

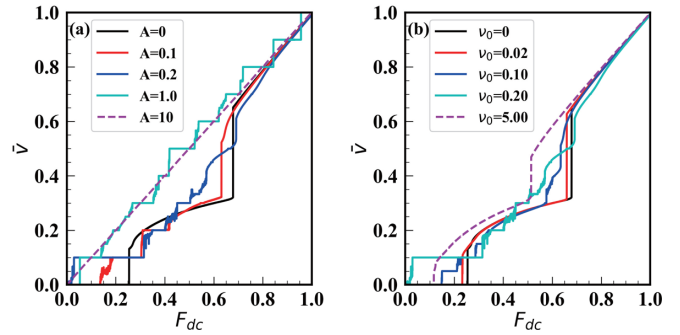


FIG. 6. Average velocity  $\bar{\nu}$  as a function of the dc force  $F_{dc}$  for  $\omega = 1/2$ ,  $K = 4$ ,  $\gamma = 1$ , in different vibration amplitude and frequency regions: (a)  $\nu_0 = 0.20$  and  $A = 0, 0.1, 0.2, 1.0, 10$  and (b)  $A = 0.2$  and  $\nu_0 = 0, 0.02, 0.10, 0.20, 5.00$ .

analogous dynamics to the dc- and ac-driven standard FK model. In the latter model, the maximum step width obtained with the change of the ac frequency is the highest one when the ac amplitude is largest, and the oscillatory behaviors of the step width appear only when the amplitude of the ac force is larger than the dynamical dc threshold value  $F_{c0}$ . Unlike the latter model, the maximum step width in the system considered is the highest one when the vibration amplitude is neither too small nor too big, and the oscillatory behaviors of the step width appear when  $F_{ac} > F_{c0}$ , where  $F_{ac}$  in Eq. (9) is influenced by both the amplitude  $A$  and the frequency  $\nu_0$ . Furthermore, in the latter model, the critical depinning forces increase and tend to the saturating value  $F_{c0}$  as the ac frequency increases. However, in the FK model with substrate lateral vibration, the critical depinning forces eventually tend to distinct values, which are smaller than  $F_{c0}$ , for different values of amplitude.

## B. Dynamic behaviors of underdamped system

In the study above, we observe that frequency locking appears in the overdamped system due to the effect of the lateral vibration, and the amplitude and frequency of the vibration have an impact on the Shapiro steps and the critical depinning force. At the same time, there is no chaos in the overdamped system, while the FK model is often accompanied by a chaotic behavior due to its discontinuous and nonintegrable characteristics [14]. Particularly, the previous research on the dc- and ac-driven standard underdamped FK model shows that chaotic behaviors occur due to the effect of inertia. Therefore, it is necessary to extend our examination of frequency locking and chaos to the underdamped FK model with substrate lateral vibration.

We take into account the underdamped system with damping coefficient  $\gamma = 1$ . Figure 6 presents the response functions  $\bar{\nu}(F_{dc})$  of Eq. (5) in the underdamped case. In Fig. 6(a) we focus on the influence of vibration amplitude on response functions when the vibration frequency is fixed as  $\nu_0 = 0.20$ . When the vibration amplitude  $A = 0$ , i.e., the underdamped FK model is driven only by the dc force, there are no dynamical mode locking, and the critical depinning force is the same as the dynamical dc threshold  $F_{c0} = 0.2545$ . When  $A = 0.1$ , we observe harmonic Shapiro steps appear, even

if there is no external ac force or radiation, which is the key factor for dynamical frequency locking. Meanwhile, the critical depinning force is greatly reduced. When  $A = 0.2$ , more harmonic steps and even subharmonic steps start to appear in the system. In addition, the first step size increases significantly while the critical depinning force almost drops to zero. When  $A = 1.0$ , there are more and more steps, harmonic and subharmonic, and the width of the first harmonic step decreases while the critical depinning force increases. Nevertheless, when the amplitude exceeds a certain range, for example  $A = 10$ , Shapiro steps disappear and the response function approaches to a linear function of the dc force. As can be seen in Fig. 6(a), as the vibration amplitude  $A$  varies, the system exhibits different dynamical behaviors, harmonic and subharmonic steps. However, when  $A$  is close to zero or extremely big, frequency-locking phenomena disappear in the system. The effect of vibration frequency on response functions for the vibration amplitude  $A = 0.2$  is shown in Fig. 6(b). Similar to the overdamped case, when the vibration frequency  $\nu_0 = 0$ , the system behaves identically to that when  $A = 0$  in Fig. 6(a). If the frequency increases to  $\nu_0 = 0.02$ , the response function curve is similar to the one of  $\nu_0 = 0$ , while the critical depinning force becomes smaller. With the further increase of frequency, a series of harmonic steps appear in the case of  $\nu_0 = 0.10$ . At the same time, the critical depinning force is further decreased. When the frequency increases to  $\nu_0 = 0.20$ , more harmonic steps and even subharmonic steps appear in the system, and the depinning force is nearly zero. If the frequency is high,  $\nu_0 = 5.00$ , the response function is similar to that of the dc-driven model, and the depinning force turns to be larger, but smaller than  $F_{c0}$ . In Fig. 6(b) we can see that the appearance of Shapiro steps depends on the vibration frequency, and if the frequency is very low or very high, there is no dynamical mode locking in the system.

### 1. Subharmonic steps and chaos in underdamped system

As depicted in Fig. 6, lateral deformation on substrate potential, that is, change of the amplitude and frequency of the vibration, affects not only the appearance of harmonic and subharmonic steps, but also their widths and the critical depinning force in the underdamped FK model. In addition to the steps, the average velocity exhibits irregular, chaotic behaviors.

In order to further explore the effect of chaotic behaviors on the harmonic and subharmonic Shapiro steps, we plot the average velocity  $\bar{v}$  as a function of the dc force and corresponding Lyapunov exponents  $\lambda_i$  for vibration amplitude  $A = 0.2$  and  $A = 1.0$  illustrated in Figs. 7 and 8, respectively. In Fig. 7(a) harmonic and subharmonic Shapiro steps, and chaos appear as the dc force increases due to the vibration introducing a new degree of freedom into the system. To verify whether the system exhibits additional subharmonic steps and hyperchaos, in Fig. 7(b) we amplify the parts that  $F_{dc} \in [0, 0.40]$  and calculate the first three largest Lyapunov exponents  $\lambda_i$ ,  $i = 1, 2, 3$ . We observe that between the steps 1 and 2, there are no subharmonic steps that are destroyed by chaos since the corresponding LLE is almost positive. And the first three largest Lyapunov exponents  $\lambda_i$ ,  $i = 1, 2, 3$  are

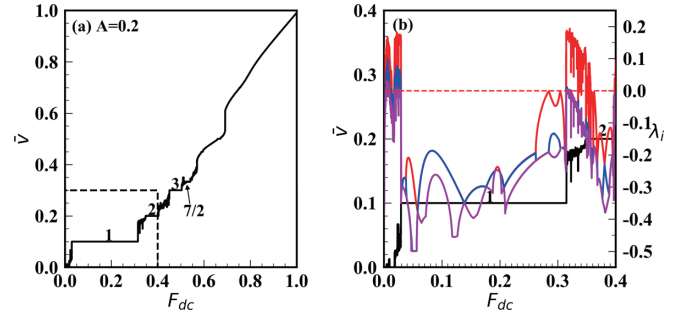


FIG. 7. (a) Average velocity  $\bar{v}$  as a function of the dc force  $F_{dc}$  for  $A = 0.2$ ,  $\nu_0 = 0.20$ . (b) Average velocity  $\bar{v}(F_{dc})$  of the selected areas of (a) and Lyapunov exponents  $\lambda_i$  as functions of the dc force. The red, blue, and magenta lines represent the first three largest Lyapunov exponents  $\lambda_1$ ,  $\lambda_2$ ,  $\lambda_3$ , respectively. The dotted line represents the curve with LLE  $\lambda = 0$ . Numbers mark Shapiro steps. The other parameters are the same as in Fig. 6.

positive for some small dc forces, indicating the occurrence of hyperchaos in the underdamped system.

When the lateral deformation is large, i.e., the vibration amplitude increases to  $A = 1.0$ , in Fig. 8(a), as the dc force increases, subharmonic steps and chaotic behaviors appear alternately between the harmonic steps. To further examine this interesting structure, we calculate Lyapunov exponents  $\lambda_i$  and focus on the region between the harmonic steps 1 and 2, which is shown in Fig. 8(b). In the response function of Fig. 8(b), a series of subharmonic steps appear, and they follow the continued fraction formula of Eq. (14). According to the Farey rule [27], the subharmonic steps are  $3/2$ ,  $5/3$ ,  $7/4$ ,  $9/5$ ,  $11/6$ ,  $\dots$ , respectively. From Figs. 7(b) and 8(b) we can conclude that the substrate potential deformation can induce the appearance of harmonic and subharmonic Shapiro steps because the latter figure with a larger amplitude of lateral vibration exhibits more steps. On the other hand, if the damping in Fig. 8(b) decreases to  $\gamma = 0.7$  while the other parameters remain unchanged, we can obtain that there is only the subharmonic step  $3/2$  between the harmonic steps 1 and 2. The decrease of damping corresponds to an increase of inertia of the system. So we can conclude that the increased inertia of the underdamped system plays an important role

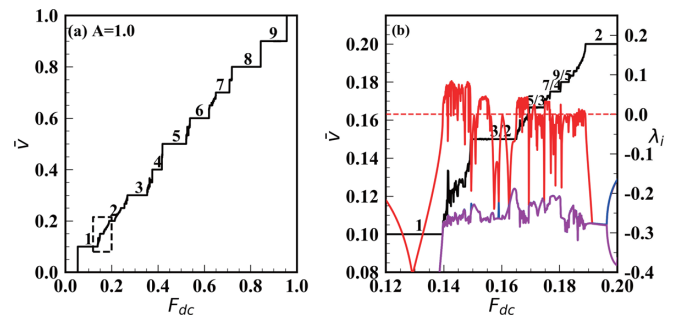


FIG. 8. (a) Average velocity  $\bar{v}$  as a function of the dc force  $F_{dc}$  for  $A = 1.0$ ,  $\nu_0 = 0.20$ . (b) Average velocity  $\bar{v}(F_{dc})$  of the selected areas in (a) and Lyapunov exponents  $\lambda_i$  as functions of the dc force. The dotted line represents the curve with LLE  $\lambda = 0$ . Numbers mark Shapiro steps. The other parameters are the same as in Fig. 6.



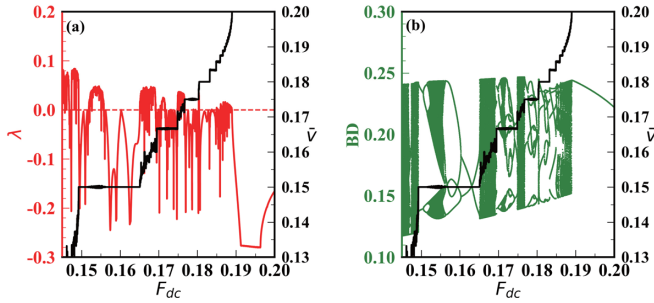


FIG. 9. (a) LLE  $\lambda$  and average velocity  $\bar{v}$  as functions of the dc force  $F_{dc}$  between the subharmonic step 3/2 and the harmonic step 2. The dotted line represents the curve with LLE  $\lambda = 0$ . (b) Bifurcation diagram (BD) of the Poincaré section corresponding to the structure in (a). The other parameters are the same as in Fig. 8.

in suppressing the emergence of subharmonic steps, which is opposite to the result of the overdamped system. Therefore, both deformation and inertia can contribute to the appearance of subharmonic steps in the underdamped FK model with substrate lateral vibration.

In Fig. 8(b) the Shapiro steps in the response function usually correspond to the regular behaviors of the system, that is, the onstep LLE is less than or equal to zero; while in between the steps, the LLE is positive, indicating that the system exhibits a chaotic behavior. However, we also observe that chaos appears on the subharmonic step 3/2 and its appearance may have an impact on the stability of the step. Further, we will study this interesting phenomenon in the high resolution with a force step  $\Delta F = 10^{-5}$ . Since the Poincaré section of the system can provide an efficient method for studying the subharmonic steps and chaotic dynamics, the high resolution plot of the LLE and the bifurcation diagram of the Poincaré section as functions of the dc force in the region between the subharmonic step 3/2 and the harmonic step 2 in Fig. 8(b) are presented in Figs. 9(a) and 9(b), respectively. The bifurcation diagram is obtained by plotting the instantaneous average velocity of particles and using the stroboscopic sampling method. For each dc force, 100 instantaneous average velocity points are plotted. In Fig. 9(a) on the subharmonic step 3/2, when the dc force is within a certain range, the LLE of the system is positive, meaning chaos appears in the system. At the same time, we can see that the chaos erodes the subharmonic step 3/2. With the increase of the dc force, the LLE becomes less than or equal to zero, which shows that the system exhibits a regular motion. Meanwhile the step returns to be stable, and it is still on the subharmonic step 3/2. The similar phenomenon also exists on other subharmonic steps, such as the subharmonic step 5/3. Looking closely at Fig. 9(b), we see that a number of bifurcation diagram curves in the regular regions are consistent with the denominator of subharmonic steps in the response function. On the subharmonic step 3/2, a series of period-doubling bifurcations occur with the increase of the dc force. Within a certain range of the dc force, these bifurcations do not alter the value of the time average mean velocity  $\bar{v}$  on the step, but when the bifurcation causes chaos to appear in the system, the time average mean velocity behaves erratically. As the dc force further increases, inverse period-doubling bifurcations appear

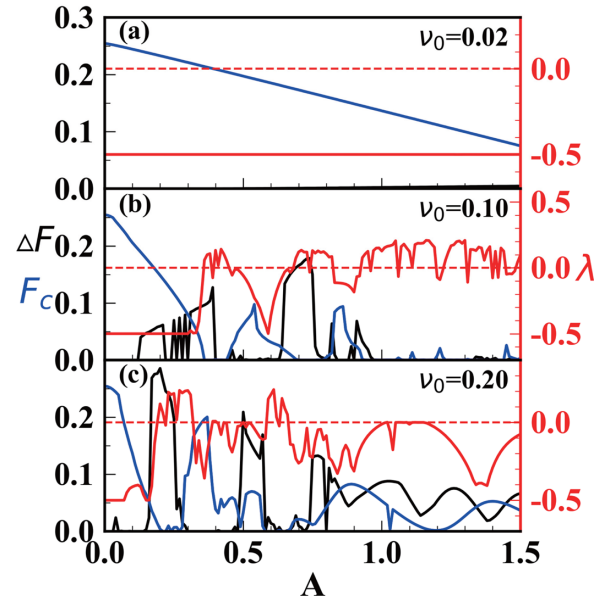


FIG. 10. The width of the first harmonic step  $\Delta F$ , the critical depinning force  $F_c$  and the LLE  $\lambda$  in the pinned state ( $F_{dc} = 0$ ) as functions of the vibration amplitude  $A$  for different values of frequency: (a)  $\nu_0 = 0.02$ , (b)  $\nu_0 = 0.10$ , (c)  $\nu_0 = 0.20$ . The dotted curve represents the curve with LLE  $\lambda = 0$ . The other parameters are the same as in Fig. 6.

and the step becomes stable again. The results indicate that the onstep chaos can affect the stability of the subharmonic steps, which should be avoided in practical applications.

## 2. Influence of vibration amplitude

In Figs. 6–9 we can observe that large subharmonic Shapiro steps and chaos appear in the underdamped system due to the lateral vibration. To further explore the influence of vibration on the system, changes of the first step width and the critical depinning force with increasing the amplitude are presented in Fig. 10 for three frequencies. Fig. 10 depicts that the influence of vibration amplitude on the first harmonic step width and the critical depinning force in the underdamped system is completely different from the one of the overdamped system in Fig. 4. At the low frequency  $\nu_0 = 0.02$  in Fig. 10(a), the first step width is nearly zero in the range of  $0 \leq A \leq 1.5$ , indicating that there is no first harmonic Shapiro step. When the frequency  $\nu_0 = 0.10$  in Fig. 10(b), the step width abruptly increases from zero when  $A \approx 0.13$ , and its values alternate between zero and nonzero as the amplitude increases. At the high frequency  $\nu_0 = 0.20$  in Fig. 10(c), the step width behaves similar to the case of  $\nu_0 = 0.10$  at the beginning of increasing amplitude, but after  $A > 0.81$ , the step width will always be larger than zero. From Fig. 10 we can conclude that the underdamped system will not show the first Shapiro step if both of amplitude and frequency are small because of zero step width, which is consistent with the result in Fig. 6. In particular, the underdamped system makes it possible for chaos to emerge, which destroys the Shapiro steps and makes the first harmonic step width no longer exhibit Bessel-type form oscillatory behaviors.

As we can see from Fig. 10, as the vibration amplitude increases, the critical depinning force  $F_c$  has different oscillation forms for three different frequency values. In Fig. 10(a), at the low frequency  $\nu_0 = 0.02$ ,  $F_c$  decreases monotonically with the increase of amplitude. When the frequency increases to  $\nu_0 = 0.10$  in Fig. 10(b),  $F_c$  first decreases monotonically to zero in the range of  $0 < A < 0.35$ . Then as the amplitude increases, all even maxima are almost zero such as the second lobe ( $0.35 < A < 0.45$ ) and the fourth lobe ( $0.69 < A < 0.80$ ), i.e., the maximum static friction force vanishes in the even lobe. That is to say, the system is in a superlubricity state, and the particles will move freely even if a very small force is applied. In Fig. 10(c) for  $\nu_0 = 0.20$ , the initial decrease of the critical depinning force becomes faster, and only a few values of  $F_c$  are zero with the increase of amplitude. Comparing with the latter two subfigures, the case of  $\nu_0 = 0.20$  is more suitable for a smaller vibration to induce superlubricity while the case of  $\nu_0 = 0.10$  allows for more possibilities of its occurrence. We observe the underdamped commensurate FK model with substrate lateral vibration exhibits the phenomenon of superlubricity that appears in the FK model with an incommensurate structure or in a two-dimensional FK model [10,49]. This is due to the effect of vibration, which causes the particles in the substrate potential to disentangle the bindings of the substrate potential and to move out of the confinement of the potential more easily. In addition, local maxima (minima) of the first step width no longer correspond to local minima (maxima) of the critical depinning force, and the mirror relationship obtained in the overdamped system between the critical depinning force and the LLE in the pinned state is completely destroyed in the underdamped case.

When  $F_{dc} = 0$ , Fig. 10(a) depicts the LLE is always negative, indicating that there is no chaos; in Fig. 10(b) chaos arises when  $A \approx 0.37$ ; in Fig. 10(c) the chaos threshold is  $A \approx 0.20$ . Thus, in the absence of the dc force, for the three frequencies considered, there is no chaotic behavior in the system if  $A$  is small. In further, we consider changing the amplitude of the lateral periodic excitations to seek a lower chaos threshold of the amplitude by setting the dc force as  $F_{dc} = 0.30$ . Figure 11 depicts the LLE of the system as a function of the amplitude of the lateral periodic excitation  $A$ . Similar to Fig. 10, we can observe that when the frequency  $\nu_0 = 0.02$  is very low, in Fig. 11(a) the system is periodic in time in the range of the amplitudes we consider; in Fig. 11(b), when  $\nu_0 = 0.10$ , chaos can appear if the amplitude is larger than the threshold of  $A \approx 0.32$ ; as the frequency increases to  $\nu_0 = 0.20$  in Fig. 11(c), the chaos threshold is  $A \approx 0.06$ , which is a small value. Comparing Figs. 11(a) and 11(b) with 11(c), we can observe that the chaos threshold of the lateral vibration amplitude becomes lower as the frequency increases. This is due to the fact that the amplitude of the ac force in Eq. (9) is not only related to the amplitude of the vibration but also to the frequency. An increase in the vibration frequency is equivalent to an increase in the amplitude of the ac force so that the chaos amplitude threshold reduces. This enlightens us that chaos in the FK model with substrate lateral vibration may be suppressed by reducing the vibration frequency to raise the chaos threshold even if the vibration is small and unavoidable.

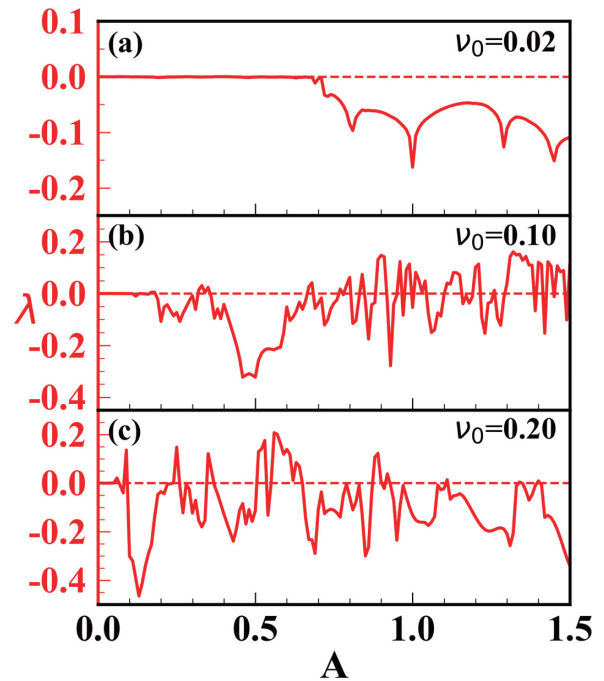


FIG. 11. LLE  $\lambda$  of the system as a function of the vibration amplitude  $A$  for different values of frequency: (a)  $\nu_0 = 0.02$ , (b)  $\nu_0 = 0.10$ , (c)  $\nu_0 = 0.20$ . The dotted line represents the curve with LLE  $\lambda = 0$ . The other parameters are the same as in Fig. 6.

### 3. Influence of vibration frequency

In Figs. 6, 10, and 11 we can see that the frequency of the vibration has a great impact on the dynamics of the system, so we explore the frequency dependence of the first step width and the critical depinning force in Fig. 12. When the vibration amplitude  $A = 0.1$  in Fig. 12(a), the first step width  $\Delta F$  is nearly zero in the region of  $0 < \nu_0 < 0.22$ , then the oscillation behavior of the step width gradually appears with the increase of frequency. When the frequency increases to  $\nu_0 \approx 0.64$ , the first harmonic step vanishes. For  $A = 0.2$  in Fig. 12(b), the step width first stays nearly zero and then changes to be greater than zero at  $\nu_0 \approx 0.03$ . As the frequency further increases, the oscillation phenomenon is similar to that in the case of  $A = 0.1$ , and the step disappears when the frequency  $\nu_0 \approx 0.65$ . In the large amplitude region  $A = 1$  in Fig. 12(c), the step width is almost zero in the range of  $0.05 < \nu_0 < 0.13$ , while with the increase of frequency, the values change from zero and are greater than zero even at high frequencies, which is different from the two previous cases, and the oscillation similar to that in Figs. 12(a) and 12(b) cannot be observed. As can be seen from Fig. 12 that in small amplitude regions, there is no first Shapiro step within the considered dc force range when the frequency is high. In Fig. 12 the critical depinning force  $F_c$  performs different behaviors with increasing frequency. In Fig. 12(a), with the increase of frequency,  $F_c$  first decreases monotonically to its minimum value, then increases to a local maximum value  $F_c \approx 0.2336$ , and finally decrease slowly, but never vanishes. In Fig. 12(b) the critical depinning force decreases monotonically to zero, and remains at zero in the interval  $\nu_0 \in [0.21, 0.26]$ , meaning that the maximum static friction vanishes in this region. Then it changes with the

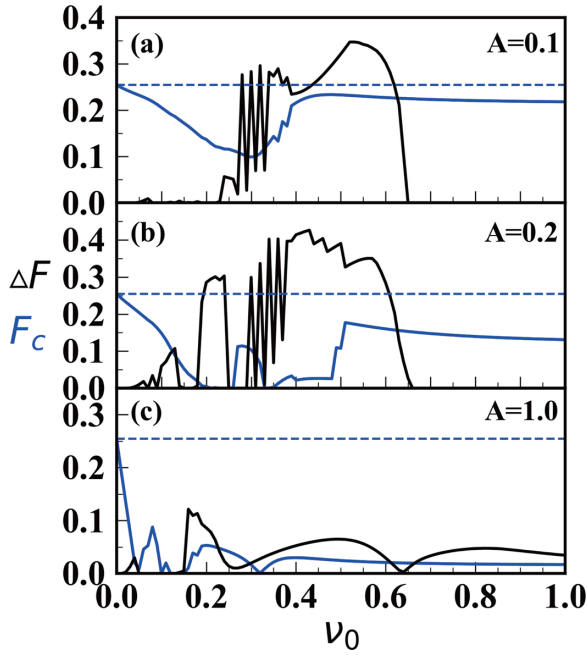


FIG. 12. The width of the first harmonic step  $\Delta F$  and the critical depinning force  $F_c$  as functions of the vibration frequency  $\nu_0$  for different values of the amplitude: (a)  $A = 0.1$ , (b)  $A = 0.2$ , (c)  $A = 1.0$ . The dotted curve represents the dynamical dc threshold:  $F_{c0} = 0.2545$ . The other parameters are the same as in Fig. 6.

increase of frequency and finally decreases gradually. When  $A = 1.0$ , the speed of  $F_c$  decreasing to zero becomes faster, and its values are zero in the frequency range of  $0.12 < \nu_0 < 0.15$ . As the frequency increases, its value eventually tends to  $F_c \approx 0.0169$ . In Fig. 12 we can see that the phenomenon of superlubricity also occurs in the system as the vibration frequency increases.

In the underdamped system, due to the presence of chaos and larger subharmonic steps, oscillations of the first step width and the critical depinning force do not follow the Bessel-type curve, and local maxima (minima) of the former no longer correspond to local minima (maxima) of the latter as depicted in Figs. 10 and 12. Meanwhile, the existence and stability of the steps are destroyed, which is related to the chaotic phenomenon in the system. Therefore, chaos must be avoided in this sense. However, the critical depinning force is nearly zero in some vibration amplitude and frequency regions, indicating that the system is likely to exhibit the phenomenon of superlubricity due to the lateral vibration. Thus, it may be possible to generate the widest Shapiro steps or the smallest static friction force by choosing an appropriate vibration amplitude and frequency in practical applications.

#### IV. CONCLUSIONS AND DISCUSSION

Using response functions, the LLE, and the bifurcation diagram of the Poincaré section, we investigate Shapiro steps and chaotic behaviors of the dc-driven FK model with substrate lateral vibration under overdamped and underdamped situations, respectively. In the overdamped situation, we show that the Shapiro steps can be generated by lateral vibration of

the substrate potential without applying an external periodic force to each particle, as the lateral vibration introduces an additional frequency and degree of freedom into the system. We can see that subharmonic Shapiro steps also appear in the model, due to the effect of inertia or deformation of the substrate potential. We show the vibration has an important effect on both the first step width and the critical depinning force. The curves of the first harmonic step width and the critical depinning force exhibit oscillatory behaviors with the increase of vibration amplitude, and local maxima of one curve correspond to local minima of the other. In particular, the step width oscillates in a Bessel-type pattern at a high frequency, while the oscillation of the critical depinning force is abnormal due to the influence of the substrate vibration. Furthermore, we observe that the dependence of the LLE on vibration amplitude in the pinned state still gives a reverse image of the amplitude dependence of the critical depinning force, further demonstrating the LLE is a very convenient tool for studying the properties of the Shapiro steps. In the frequency dependence, when the vibration amplitude is large, the step width and the critical depinning force oscillate at low frequencies, while the oscillatory behaviors vanish as the frequency increases. In contrast to the overdamped system, the underdamped one exhibits large subharmonic Shapiro steps and chaotic behaviors. We show the increased inertia of the latter system plays an important role in suppressing the emergence of subharmonic steps, which is opposite to the result of the former. In a relatively large amplitude value, large subharmonic steps and chaotic behaviors appear alternately between the harmonic steps, and the appearance of the subharmonic steps follows the Farey rule. By using the LLE and the bifurcation diagram of the Poincaré section, we see that the onstep chaos can destroy the stability of the steps. Due to the appearance of large subharmonic steps and chaos, the amplitude and frequency dependence of the first step width and the critical depinning force in the underdamped system, do not follow the same laws as the overdamped one, exhibiting more complicated behaviors. We show the step width is nearly zero in some vibration amplitude and frequency regions, and the critical depinning force almost vanishes, which gives rise to superlubricity. We also observe that the reverse image between the amplitude dependence of the depinning force and LLE in the pinned state vanishes, and the chaos threshold of the vibration amplitude becomes lower when the frequency increases.

The findings may have important implications for nonlinear physical systems which have competing frequencies, such as charge- or spin-density wave systems, Josephson junction systems, and vortex lattices. Although these systems may have physical, chemical, and biological origins, their dynamics are commonly characterized by equations similar to those used in this study. The dependence of the first harmonic step width and the critical depinning force on the amplitude and frequency of the substrate vibration allows us to select the appropriate amplitude and frequency to obtain the maximum step width to take better advantage of the synchronization phenomenon or realize a voltage standard in different devices [50], and to obtain the minimum critical depinning force to reduce nanofriction and avoid wear of mechanical equipment. Moreover, the mirror relationship between the LLE in the

pinned state and the critical depinning force is highly useful to both theoretical and experimental studies, particularly in systems where only averaged or integrated quantities like current and voltage can be measured [22]. When the system changes from the overdamped case to the underdamped one, large subharmonic steps and chaos occur. In recent years, research in Josephson junctions has paid particular attention to the existence of structural chaos [44,51], and we observe a similar phenomenon in this work. However, the onstep chaos leads to the destruction of the stability of the subharmonic steps, which may affect the accuracy of Majorana fermions detection, since the signature of the Majorana states can be represented by a specific sequence of subharmonic steps [52]. Also, in voltage standards or other applications, the optimum operating region

is actually close to the onset of chaos, indicating that the chaotic behaviors must be avoided [53]. Therefore, the reason for the emergence of chaos in the system and how to control it deserves further study in future research.

### ACKNOWLEDGMENTS

We would like to thank the anonymous reviewers for their constructive comments and suggestions which helped us to improve the quality of the paper. We would also like to thank Q. Hou for improving the English of the paper. This work is supported by the National Natural Science Foundation of China (Grant No. 12072262).

- 
- [1] S. Shapiro, Josephson Currents in Superconducting Tunneling: The Effect of Microwaves and other Observations, *Phys. Rev. Lett.* **11**, 80 (1963).
- [2] S. A. Nikonov, S. G. Zybtsev, and V. Y. Pokrovskii, RF wave mixing with sliding charge-density waves, *Appl. Phys. Lett.* **118**, 253108 (2021).
- [3] G. Kriza, G. Quirion, O. Traetteberg, W. Kang, and D. Jérôme, Shapiro Interference in a Spin-Density-Wave System, *Phys. Rev. Lett.* **66**, 1922 (1991).
- [4] I. R. Rahmonov, J. Tekić, P. Mali, A. Irie, and Y. M. Shukrinov, ac-driven annular Josephson junctions: The missing Shapiro steps, *Phys. Rev. B* **101**, 024512 (2020).
- [5] N. Kokubo, R. Besseling, and P. H. Kes, Dynamic ordering and frustration of confined vortex rows studied by mode-locking experiments, *Phys. Rev. B* **69**, 064504 (2004).
- [6] J. Ridderbos, M. Brauns, A. Li, E. P. Bakkers, A. Brinkman, W. G. Van Der Wiel, and F. A. Zwanenburg, Multiple Andreev reflections and Shapiro steps in a Ge-Si nanowire Josephson junction, *Phys. Rev. Mater.* **3**, 084803 (2019).
- [7] N. P. Vizir, C. J. O. Reichhardt, P. A. Venegas, and C. Reichhardt, Skyrmion dynamics and transverse mobility: Skyrmion Hall angle reversal on 2D periodic substrates with dc and biharmonic ac drives, *Eur. Phys. J. B* **93**, 112 (2020).
- [8] M. P. N. Juniper, A. V. Straube, R. Besseling, D. G. A. L. Aarts, and R. P. A. Dullens, Microscopic dynamics of synchronization in driven colloids, *Nat. Commun.* **6**, 7187 (2015).
- [9] T. Kontorova and J. Frenkel, On the theory of plastic deformation and twinning, II, *Zh. Eksp. Teor. Fiz.* **8**, 1340 (1938).
- [10] N. Manini, O. M. Braun, E. Tosatti, R. Guerra, and A. Vanossi, Friction and nonlinear dynamics, *J. Phys. Condens. Matter* **28**, 293001 (2016).
- [11] A. Vanossi, G. Santoro, and V. Bortolani, Hysteretic behaviour in driven Frenkel-Kontorova chains on irregular substrates, *J. Phys. Condens. Matter* **16**, S2895 (2004).
- [12] Y. M. Lei, F. Zheng, and X. Z. Shao, Chaos and chaos control of the Frenkel-Kontorova model with dichotomous noise, *Int J Bifurcat Chaos* **27**, 1750052 (2017).
- [13] L. M. Floría and J. J. Mazo, Dissipative dynamics of the Frenkel-Kontorova model, *Adv. Phys.* **45**, 505 (1996).
- [14] O. M. Braun and Y. S. Kivshar, *The Frenkel-Kontorova Model: Concepts, Methods, and Applications* (Springer, Berlin, 2004).
- [15] L. M. Floría, C. Baesens, and J. Gómez-Gardenes, in *Dynamics of Coupled Map Lattices and of Related Spatially Extended Systems* (Springer, Berlin, 2005).
- [16] J. Tekić and P. Mali, *The ac Driven Frenkel-Kontorova Model* (University of Novi Sad, Novi Sad, 2015).
- [17] A. Vanossi, A. R. Bishop, and V. Bortolani, Role of substrate geometry in sliding friction, *Nanotechnology* **15**, 790 (2004).
- [18] L. P. Jia, J. Tekić, Y. Yang, C. L. Wang, W. S. Duan, and L. Yang, Friction phenomena in the overdamped three-layer model, *Phys. Rev. E* **91**, 022911 (2015).
- [19] F. Falo, L. M. Floría, P. J. Martínez, and J. J. Mazo, Unlocking mechanism in the ac dynamics of the Frenkel-Kontorova model, *Phys. Rev. B* **48**, 7434 (1993).
- [20] L. M. Floría and F. Falo, Shapiro Steps in the Steady-State Dynamics of Incommensurate Structures, *Phys. Rev. Lett.* **68**, 2713 (1992).
- [21] B. B. Hu and J. Tekić, Amplitude and frequency dependence of the Shapiro steps in the dc- and ac-driven overdamped Frenkel-Kontorova model, *Phys. Rev. E* **75**, 056608 (2007).
- [22] J. Odavić, P. Mali, J. Tekić, M. Pantić, and M. Pavkov-Hrvojević, Application of largest Lyapunov exponent analysis on the studies of dynamics under external forces, *Commun. Nonlin. Sci. Numer. Sim.* **47**, 100 (2017).
- [23] M. J. Renné and D. Polder, Some analytical results for the resistively shunted Josephson junction, *Rev. Phys. Appl.* **9**, 25 (1974).
- [24] J. R. Waldram and P. H. Wu, An alternative analysis of the nonlinear equations of the current-driven Josephson junction, *J. Low Temp. Phys.* **47**, 363 (1982).
- [25] R. Hilborn, *Chaos and Nonlinear Dynamics: An Introduction for Scientists and Engineers*, 2nd ed. (Oxford University Press, Oxford, 2001).
- [26] S. Gombar, P. Mali, S. Radošević, J. Tekić, M. Pantić, and M. Pavkov-Hrvojević, Influence of anharmonic convex interparticle potential and Shapiro steps in the opposite direction of driving force, *Phys. Scr.* **96**, 035211 (2021).
- [27] J. Odavić, P. Mali, and J. Tekić, Farey sequence in the appearance of subharmonic Shapiro steps, *Phys. Rev. E* **91**, 052904 (2015).
- [28] J. Tekić and B. B. Hu, Properties of the Shapiro steps in the ac driven Frenkel-Kontorova model with deformable substrate potential, *Phys. Rev. E* **81**, 036604 (2010).

- [29] P. Mali, J. Tekić, and M. Pantić, Saturation effects in ac + dc driven Frenkel–Kontorova model, *Commun. Nonlin. Sci. Numer. Sim.* **19**, 3469 (2014).
- [30] I. Sokolović, P. Mali, J. Odavić, S. Radošević, S. Y. Medvedeva, A. E. Botha, Y. M. Shukrinov, and J. Tekić, Devil’s staircase and the absence of chaos in the dc- and ac-driven overdamped Frenkel-Kontorova model, *Phys. Rev. E* **96**, 022210 (2017).
- [31] C. L. Wang, J. Tekić, W. S. Duan, Z. G. Shao, and L. Yang, Existence and stability of the resonant phenomena in the dc- and ac-driven overdamped Frenkel-Kontorova model with the incommensurate structure, *Phys. Rev. E* **84**, 046603 (2011).
- [32] A. A. Middleton, Asymptotic Uniqueness of the Sliding State for Charge-Density Waves, *Phys. Rev. Lett.* **68**, 670 (1992).
- [33] A. A. Middleton and D. S. Fisher, Critical behavior of charge-density waves below threshold: Numerical and scaling analysis, *Phys. Rev. B* **47**, 3530 (1993).
- [34] J. Tekić, A. E. Botha, P. Mali, and Y. M. Shukrinov, Inertial effects in the dc + ac driven underdamped Frenkel-Kontorova model: Subharmonic steps, chaos, and hysteresis, *Phys. Rev. E* **99**, 022206 (2019).
- [35] J. Tekić, A. Botha, P. Mali, and Y. M. Shukrinov, in *13th Chaotic Modeling and Simulation International Conference*, edited by C. H. Skiadas and Y. Dimotikalis (Springer International Publishing, Cham, 2021), p. 943.
- [36] M. A. Karami and D. J. Inman, Equivalent damping and frequency change for linear and nonlinear hybrid vibrational energy harvesting systems, *J. Sound Vib.* **330**, 5583 (2011).
- [37] R. Chacón, P. J. Martínez, and J. A. Martínez, Dissipative dynamics of a particle in a vibrating periodic potential: Chaos and control, *Phys. Rev. E* **92**, 062921 (2015).
- [38] Y. Azizi and A. Valizadeh, Rectified motion of a Bose-Einstein condensate in a horizontally vibrating shallow optical lattice, *Phys. Rev. A* **83**, 013614 (2011).
- [39] Z. Tshiprut, A. E. Filippov, and M. Urbakh, Tuning Diffusion and Friction in Microscopic Contacts by Mechanical Excitations, *Phys. Rev. Lett.* **95**, 016101 (2005).
- [40] Z. Tshiprut, A. E. Filippov, and M. Urbakh, The effect of lateral vibrations on transport and friction in nanoscale contacts, *Tribol. Int.* **40**, 967 (2007).
- [41] R. Guerra, A. Vanossi, and M. Urbakh, Controlling microscopic friction through mechanical oscillations, *Phys. Rev. E* **78**, 036110 (2008).
- [42] M. Ma, I. M. Sokolov, W. Wang, A. E. Filippov, Q. S. Zheng, and M. Urbakh, Diffusion through Bifurcations in Oscillating Nano- and Microscale Contacts: Fundamentals and Applications, *Phys. Rev. X* **5**, 031020 (2015).
- [43] Y. M. Shukrinov, S. Y. Medvedeva, A. E. Botha, M. R. Kolahchi, and A. Irie, Devil’s staircases and continued fractions in Josephson junctions, *Phys. Rev. B* **88**, 214515 (2013).
- [44] Y. M. Shukrinov, A. E. Botha, S. Y. Medvedeva, M. R. Kolahchi, and A. Irie, Structured chaos in a devil’s staircase of the Josephson junction, *Chaos* **24**, 033115 (2014).
- [45] P. Mali, A. Šakota, J. Tekić, S. Radošević, M. Pantić, and M. Pavkov-Hrvojević, Complexity of Shapiro steps, *Phys. Rev. E* **101**, 032203 (2020).
- [46] A. Wolf, J. B. Swift, H. L. Swinney, and J. A. Vastano, Determining Lyapunov exponents from a time series, *Physica D* **16**, 285 (1985).
- [47] R. E. Thorne, J. S. Hubacek, W. G. Lyons, J. W. Lyding, and J. R. Tucker, ac-dc interference, complete mode locking, and origin of coherent oscillations in sliding charge-density-wave systems, *Phys. Rev. B* **37**, 10055 (1988).
- [48] R. E. Thorne, W. G. Lyons, J. W. Lyding, J. R. Tucker, and J. Bardeen, Charge-density-wave transport in quasi-one-dimensional conductors. II. ac-dc interference phenomena, *Phys. Rev. B* **35**, 6360 (1987).
- [49] C.-L. Wang, W.-S. Duan, X.-R. Hong, and J.-M. Chen, Investigation of superlubricity in a two-dimensional Frenkel–Kontorova model with square lattice symmetry, *Appl. Phys. Lett.* **93**, 153116 (2008).
- [50] W. Buckel and R. Kleiner, *Superconductivity: Fundamentals and Applications* (Wiley, New York, 2008).
- [51] A. E. Botha, Y. M. Shukrinov, S. Y. Medvedeva, and M. R. Kolahchi, Structured chaos in 1-D stacks of intrinsic Josephson junctions irradiated by electromagnetic waves, *J. Supercond. Nov. Magn.* **28**, 349 (2014).
- [52] M. Maiti, K. V. Kulikov, K. Sengupta, and Y. M. Shukrinov, Josephson junction detectors for Majorana modes and Dirac fermions, *Phys. Rev. B* **92**, 224501 (2015).
- [53] R. L. Kautz, Noise, chaos, and the Josephson voltage standard, *Rep. Prog. Phys.* **59**, 935 (1996).